RSC Advances

PAPER

View Article Online
View Journal | View Issue

Cite this: *RSC Adv.*, 2019, **9**, 4172

Enhancement of protein stability by an additional disulfide bond designed in human neuroglobin†

Hai-Xiao Liu,[a] Lianzhi Li,[b] Xin-Zhi Yang,[c] Chuan-Wan Wei,[a] Hui-Min Cheng,[a] Shu-Qin Gao,[c] Ge-Bo Wen[c] and Ying-Wu Lin *[ac]

Human neuroglobin (Ngb) forms an intramolecular disulfide bond between Cys46 and Cys55, with a third Cys120 near the protein surface, which is a promising protein model for heme protein design. In order to protect the free Cys120 and to enhance the protein stability, we herein developed a strategy by designing an additional disulfide bond between Cys120 and Cys15 *via* A15C mutation. The design was supported by molecular modeling, and the formation of Cys15–Cys120 disulfide bond was confirmed experimentally by ESI-MS analysis. Molecular modeling, UV-Vis and CD spectroscopy showed that the additional disulfide bond caused minimal structural alterations of Ngb. Meanwhile, the disulfide bond of Cys15–Cys120 was found to enhance both Gdn·HCl-induced unfolding stability (increased by ~0.64 M) and pH-induced unfolding stability (decreased by ~0.69 pH unit), as compared to those of WT Ngb with a single native disulfide bond of Cys46–Cys55. Moreover, the half denaturation temperature (T_m) of A15C Ngb was determined to be higher than 100 °C. In addition, the disulfide bond of Cys15–Cys120 has slight effects on protein function, such as an increase in the rate of O_2 release by ~1.4-fold. This study not only suggests a crucial role of the artificial disulfide in protein stabilization, but also lays the groundwork for further investigation of the structure and function of Ngb, as well as for the design of other functional heme proteins, based on the scaffold of A15C Ngb with an enhanced stability.

Received 19th December 2018
Accepted 28th January 2019

DOI: 10.1039/c8ra10390a

rsc.li/rsc-advances

Introduction

Metalloproteins and metalloenzymes play crucial roles in biological systems, including electron transfer, gas transport, and catalysis.[1–6] In order to expand their functionalities, researchers have made great efforts in the design of artificial metalloproteins and metalloenzymes.[1,7–17] Since enzyme activity is affected by many factors, increasing the protein stability may ensure the artificial enzymes to be active under harsh reaction conditions, such as in presence of denaturing agents, with high temperature and in different pH solutions. For this purpose, various strategies have been developed in the last decade, such as rational design,[18] directed evolution,[19] and computational design,[20] by improving the hydrophobic and hydrogen(H)-bonding interactions within the protein scaffold. Moreover, covalent interactions such as disulfide bonds play a crucial role in protein stabilization, and design of *de novo* disulfide bond has shown to be useful for enhancing the protein stability.[21–27]

Heme proteins are a major class of metalloproteins and metalloenzymes.[4] To increase the protein stability, especially for the heme-binding affinity of heme proteins, a common approach is to construct a covalent heme to protein cross-link, as occurred in natural cytochrome *c* (Cyt *c*) and some Cyt P450s.[28–30] For example, a Cyt *c*-like covalent link (Cys-heme cross-link) has been constructed in Cyt b_5,[31–33] Cyt b_{562},[34] ascorbate peroxidase,[35] and myoglobin (Mb).[36] Moreover, other heme-protein cross-links such as Met-Heme,[37] His-Heme,[38] and Tyr-heme,[39,40] can also be designed in artificial heme proteins. In addition to heme-protein cross-links, design of *de novo* disulfide bond has shown to be powerful, not only to increase the protein stability but also fine-tune the reactivity of heme proteins.[30] For example, Morishima and co-workers constructed a *de novo* disulfide bond in Mb that was found to affect ligand binding dynamics.[41] In recent studies, we designed a *de novo* disulfide bond in Mb, which enhances both protein stability toward guanidine hydrochloride (Gdn·HCl)-inducing unfolding, and reactivity, such as peroxidase and nitrite reductase activities.[42,43]

Neuroglobin (Ngb) was discovered in 2000 as a new member of globins, highly expressed in nerve tissues.[44] In addition to the feature of a bis-His (His64/His96) heme coordination, human Ngb forms an intramolecular disulfide bond (Cys46–Cys55), which regulates the coordination of His64 and the binding of exogenous ligands, such as O_2 and CO, to the heme iron.[45–48]

[a]*School of Chemistry and Chemical Engineering, University of South China, Hengyang 421001, China. E-mail: linlinying@hotmail.com; ywlin@usc.edu.cn*

[b]*School of Chemistry and Chemical Engineering, Liaocheng University, Liaocheng 252059, China*

[c]*Laboratory of Protein Structure and Function, University of South China, Hengyang 421001, China*

† Electronic supplementary information (ESI) available: Additional UV-Vis, CD and stopped-flow spectra. See DOI: 10.1039/c8ra10390a

Moreover, human Ngb has a third cysteine (Cys120), which is located near the protein surface, and is thus prone to be modified by reactive oxygen/nitrogen species (ROS/RNS) in oxidative stress conditions.[49] The single free Cys120 near the protein surface may also lead to protein dimerization in purification of the recombinant Ngb protein. Therefore, Cys120 was usually replaced by a Ser to simplify protein purification and prevent protein dimerization, and functional studies were performed based on the C120S Ngb mutant.[50–52] Meanwhile, Ser120 forms an H-bonding network with His23 and Glu22 that is missing in wild-type (WT) Ngb, which may affect ligand migration from the protein matrix.[53] Although Cys120 has a biological role and contributes to the interface between helix G and the A–B loop, from a perspective of heme protein design and application, Ngb is a promising model protein. For example, H64Q Ngb can be a ligand-trap antidote for CO poisoning in practical medicine,[54] and H64A Ngb is an artificial nitrite reductase with the fastest reported activity.[55]

With a motivation to design Ngb mutants with advanced properties and potential applications, we anticipate that if an intramolecular disulfide bond could be constructed between Cys120 and another Cys introduced nearby, Cys120 might be protected, and the protein stability could be enhanced as well. To this end, we inspected the X-ray structure of human Ngb (PDB code 4MPM[48]), and found that Ala15 was a potential target for introducing a Cys residue, which was further supported by molecular modeling studies. As shown in this study, we found that Cys15 could indeed form an intramolecular disulfide with Cys120, as confirmed by protein mass spectrometry analysis. The additional disulfide bond (C15–C120) in A15C Ngb mutant was found to enhance both chemical and pH stabilities compared to those of WT Ngb with a single disulfide bond (C46–C55). Moreover, the thermal stability of A15C Ngb was found to be more than 100 °C, suggesting a crucial role of C15–C120 in protein stabilization.

Results and discussion

Molecular modeling studies

In order to construct an additional disulfide bond in human Ngb to protect Cys120 and stabilize the protein, we inspected the X-ray structure of human Ngb and found that Ala15 was a potential target for introducing a Cys residue. To reveal the possibility of formation of a disulfide bond between C15 and C120, we first performed a molecular modeling study for A15C Ngb with two intramolecular disulfide bonds. With minimization and equilibration, the simulated structure of A15C Ngb (Fig. 1A) showed that the two disulfide bonds could be well formed, with a disulfide bond distance of 2.11 Å (C15–C120) and 2.05 Å (C46–C55), respectively, in agreement with the X-ray structure of WT Ngb (2.02 Å for C46–C55).[48] Moreover, as shown in Fig. 1B, the structure overlapped well with the X-ray structure of WT Ngb, which suggests that the formation an disulfide bond of C15–C120 causes minimal structural alterations.

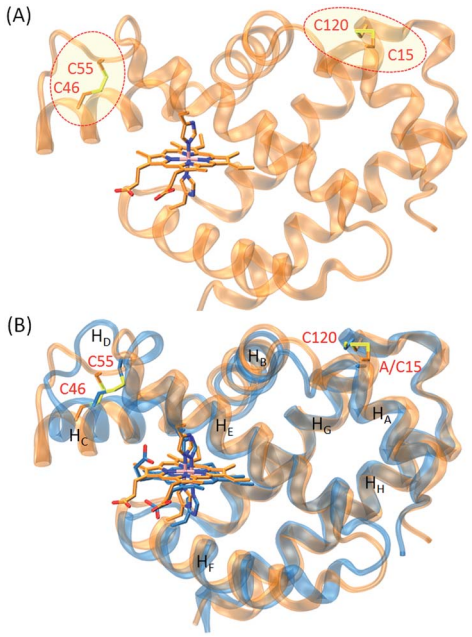

Fig. 1 (A) Modeling structure of A15C Ngb, showing the disulfide bonds (indicated by circle lines), and (B) overlaid with the X-ray structure of WT Ngb (blue), with the secondary structures of H_A–H_H labeled.

Spectroscopic studies

With support by molecular modeling, we introduced an additional Cys residue at position 15 in Ngb by A15C mutation. The A15C Ngb mutant was expressed and purified using the same procedure as that for WT Ngb. UV-Vis studies showed that A15C Ngb exhibits the spectra (ferric, 413, 532 and 562 nm; ferrous, 425, 529 and 559 nm, Fig. 2A) with the maximum absorbance identical to those of WT Ngb in both ferric and ferrous states (Fig. S1†).[45,56] Moreover, A15C Ngb was found to exhibit the CD spectrum almost identical to that of WT Ngb (Fig. 2B). These observations suggest that introduction of Cys15 does not alter the heme coordination state and the protein secondary structure.

To reveal whether Cys15 forms an intramolecular with Cys120 in A15C Ngb, we performed mass spectrometry studies using an electrospray ionization (ESI) technique, with WT Ngb as controls. As shown in Fig. 3A, the mass spectrum of WT Ngb exhibits a mass of 16 931.5 Da, in agreement with previous observation for oxidized Ngb (16 930.9 Da),[46] which corresponds to the apo-protein of WT Ngb with an intramolecular disulfide bond (Cys46–Cys55) (calculated, 16 931 Da). Note that the heme was dissociated under the detection conditions. Upon treatment by TCEP, a mass of 16 933.5 Da was observed, with an increase mass of 2 Da, which indicates the reduction of disulfide bond of Cys46–Cys55, as shown for reduced Ngb (16 932.2 Da).[46] In the mass spectrum of A15C Ngb (Fig. 3B), it was interesting to observe two mass peaks (16 961.5 D and 17 576.5 Da), which correspond to the calculated apo-protein of A15C Ngb with two intramolecular disulfide bonds (16 961 Da), and the holo-protein with heme not dissociated (17 576 Da),

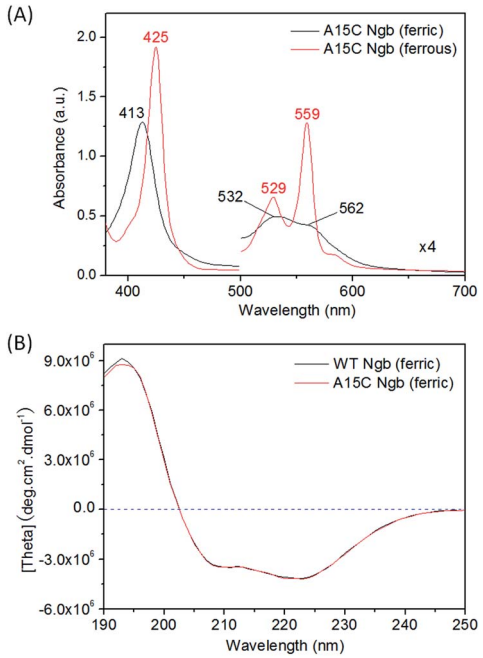

Fig. 2 Spectroscopic properties of A15C Ngb. (A) UV-Vis spectra in both oxidation states, and (B) CD spectrum in ferric state (10 μM protein in 100 mM potassium phosphate buffer, pH 7.0, 25 °C), with WT Ngb shown for comparison.

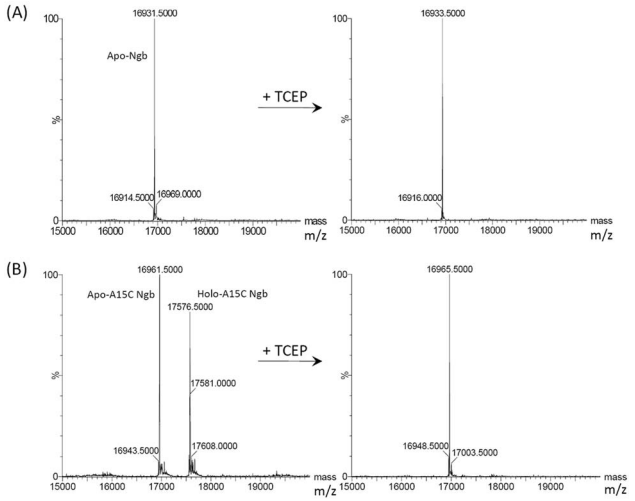

Fig. 3 ESI-MS analysis of WT Ngb (A) and A15C Ngb (B) as purified (left) and treated with reducing agent TCEP (right).

respectively. After treatment with TCEP, a single mass of 16 965.5 Da of the apo-protein was observed, with an increase mass of 4 Da, suggesting the reduction of two intramolecular disulfide bonds. The disappearance of mass peak for the holo-protein upon TCEP treatment also suggested that the heme dissociated from the protein matrix in mass determination, which, in turn, suggested that the formation of two intramolecular disulfide bonds, C46–C55 and C15–C120, may enhance the heme-binding stability of A15C Ngb under these conditions.

Chemical-induced unfolding studies

Since it is not possible to investigate A15C Ngb with one disulfide bond intact and the other cleaved, to probe the contribution of an additional disulfide bond of C15–C120 to the protein chemical stability, we first performed Gdn·HCl-induced unfolding studies for both A15C Ngb and WT Ngb. As shown in Fig. 4A and S2,† the intensity of Soret band (413 nm) of both proteins decreased with increasing the concentration of Gdn·HCl to 6 M, and resulted in a shoulder peak at ~370 nm. Concurrently, the visible bands (532 nm and 562 nm) of bis-His coordinated heme decreased with an appearance of ~630 nm. These observations suggest the release of heme from the heme pocket upon protein unfolding. Moreover, there was an isosbestic point observed in both UV-Vis spectroscopic changes, which indicates that the Gdn·HCl-induced unfolding was a two-state process for both proteins.

To compare the half denaturation concentration (C_m), we plotted the spectral changes of the Soret band *versus* the concentration of Gdn·HCl and fitted to a normalized two-state model (Fig. 4B). The results showed that A15C Ngb exhibited a C_m value of 4.39 ± 0.01 M, which is ~0.64 M higher than that of WT Ngb (3.75 ± 0.01 M). This observation suggest that the disulfide bond of C15–C120 in A15C Ngb enhances the protein chemical stability of Gdn·HCl-induced unfolding. Remarkably, the enhancement of ~0.64 M is much larger than that of a disulfide bond constructed in other heme proteins. For example, we observed an increase of ~0.32 M for V21C/V66C Mb, with a disulfide bond mimicking that in cytoglobin (Cgb), as compared to that of WT Mb upon Gdn·HCl-inducing

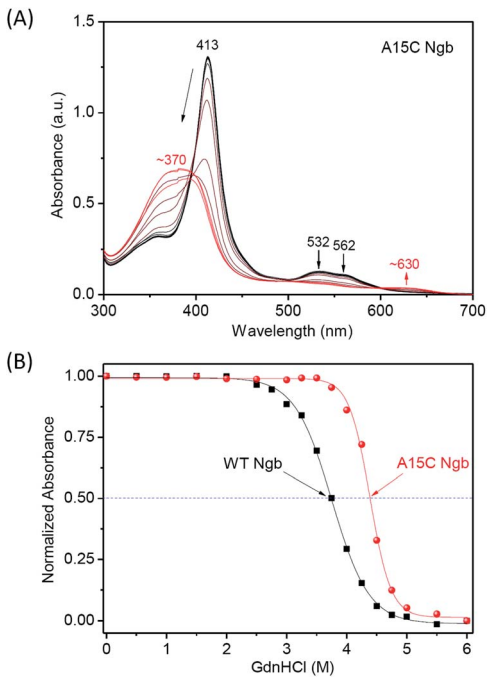

Fig. 4 UV-Vis spectra of Gdn·HCl-induced unfolding of (A) A15C Ngb (10 μM protein in 100 mM potassium phosphate buffer, pH 7.0). (B) Normalized absorbance of the Soret band *versus* Gdn·HCl concentrations.

unfolding.[43] Fasan and co-workers showed that construction of an artificial thioether bond between a non-natural amino acid of O-2-bromoethyl Tyr and Cys in Mb may increase ~0.24 M for C_m upon Gdn·HCl-induced unfolding.[57] Moreover, Hollenberg and co-workers constructed a *de novo* disulfide bond close to the heme center in Cyt P450 2B1 by a double mutation of Y309C/S360C, which reduced the protein plasticity and fine-tuned the metabolic activity.[58] These observations suggest that the location for engineering a covalent bond is crucial for the enhancement of stability, as well as functional regulation.

To further evaluate the chemical stability of A15C Ngb, we performed an acid titration experiment, and compared to that of WT Ngb under the same conditions. It was shown that by titration of concentrated HCl into the protein solution, the Soret band decreased and shifted to ~370 nm, as well as for the visible bands (Fig. 5A and S3†). The spectral changes were similar to those occurred for Gdn·HCl-induced unfolding, with appearance of an isosbestic point, which indicates that acid-induced unfolding of both proteins was also a two-state process. This was further confirmed by the well-fitting of the plots of Soret band changes *versus* the pH values (Fig. 5B). The results showed that the half denaturation pH value was decreased by ~0.69 pH unit for A15C Ngb (2.62 ± 0.02) compared to that of WT Ngb (3.31 ± 0.01), which indicates that the formation of an additional disulfide bond of C15–C120 increases the acid tolerance of A15C Ngb.

Thermal-induced unfolding studies

In addition to the protein chemical stability, we investigated the thermal stability of A15C Ngb, with WT Ngb as a control. We first performed the far-UV CD spectroscopy studies to monitor the changes in secondary structure upon increasing temperature. As shown in Fig. 6A and S4† with the temperature increasing from 25 °C to 100 °C, the negative Cotton effects at 208 nm and 222 nm gradually decreased, suggesting the unfolding of α-helix structure. When the temperature reached 100 °C, ~50% α-helix was retained in A15C Ngb, while less than 25% was observed for WT Ngb. The plot of absorbance at 220 nm *versus* temperature showed that WT Ngb exhibits a half denaturation temperature (T_m) of 88.5 °C (Fig. 6B). Note that since A15C Ngb was only partially unfolded at 100 °C, T_m could not be determined and was estimated to be higher than 100 °C. These observations thus suggest that the second disulfide bond of C15–C120 stabilizes the secondary structure of A15C Ngb.

Moreover, we monitored the UV-Vis spectral changes upon increasing temperature (Fig. 7), which provides valuable information for the heme binding and the overall protein structure. The results showed that with the temperature increasing from 25 °C to 100 °C, the Soret band of WT Ngb gradually decreased from 413 nm and blue shifted to ~398 nm, with disappearance of visible bands at 532 nm and 562 nm (Fig. 7A). The isosbestic point also indicated that the thermal-induced unfolding of WT Ngb was a two-state process. The spectral changes were similar to those of Gdn·HCl or acid-induced unfolding, whereas the ultimate spectrum was different, with a Soret band of ~398 nm instead of ~370 nm of the free heme. These observations suggest that although the heme was released from the heme pocket at high temperature, it was still associated with the protein peptide. The plot of Soret band at 413 nm *versus* temperature showed that WT Ngb exhibits a half denaturation

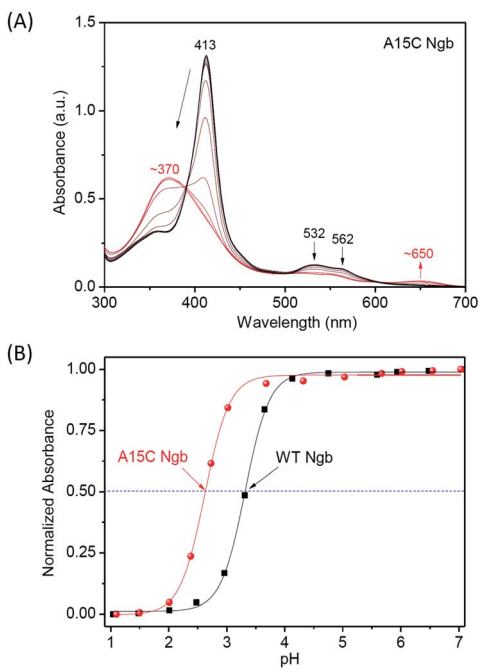

Fig. 5 UV-Vis spectra of acid-induced unfolding of (A) A15C Ngb (10 μM). (B) Normalized absorbance of the Soret band *versus* pH values.

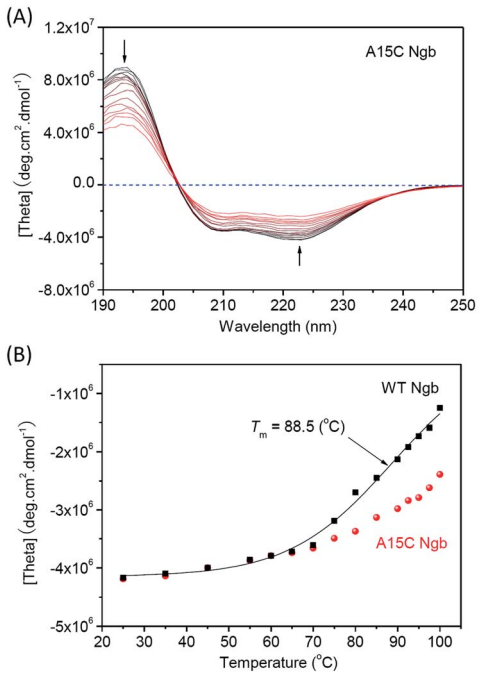

Fig. 6 CD spectra of thermal-induced unfolding of (A) A15C Ngb (10 μM protein in 100 mM potassium phosphate buffer, pH 7.0). (B) Plots of absorbance at 222 nm *versus* temperature.

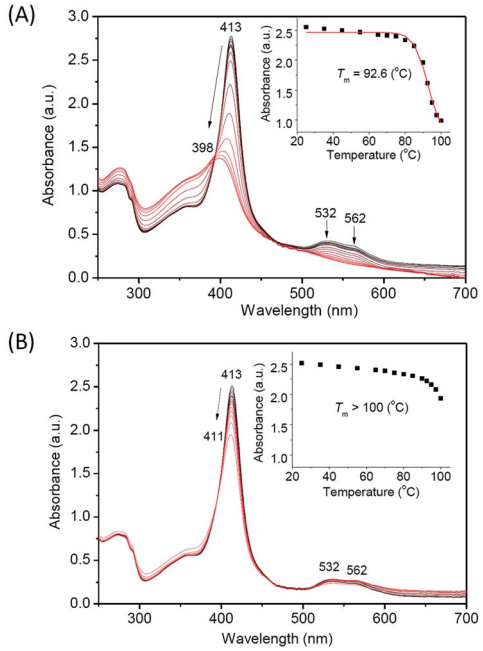

Fig. 7 UV-Vis spectra of thermal-induced unfolding of (A) WT Ngb and (B) A15C Ngb (10 μM protein in 100 mM potassium phosphate buffer, pH 7.0). The plot of Soret band at 413 nm *versus* temperature was shown as an inset.

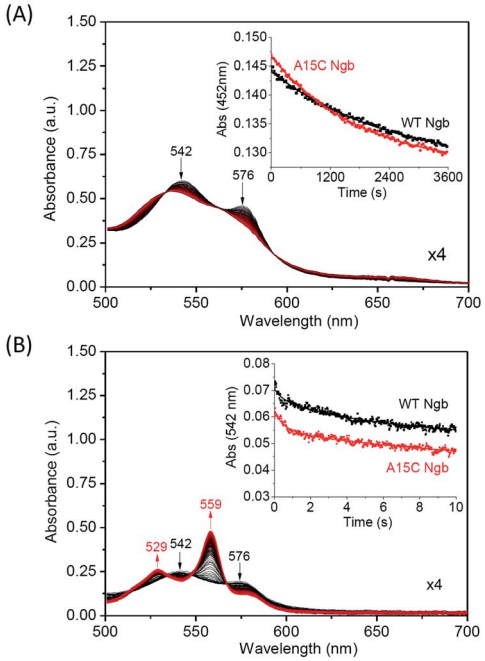

Fig. 8 (A) UV-Vis spectra of autoxidation of oxy-A15C Ngb (10 μM protein in 100 mM potassium phosphate buffer, pH 7.0) for 60 min at 25 °C. (B) Stopped-flow spectra of oxy-A15C Ngb (5 μM protein in 100 mM potassium phosphate buffer, pH 7.0), in reaction with 1 mM dithionite in the same buffer for 10 s at 25 °C. The time dependent changes for the oxy-form at 542 nm were shown as insets, with WT Ngb under the same conditions shown for comparison.

temperature (T_m) of 92.6 °C (Fig. 7A, inset). Note that this value is ~4 °C higher than that determined by monitoring the changes in secondary structure, suggesting a more stability for the heme active center. In contrast to WT Ngb, A15C Ngb underwent only partial unfolding when the temperature was increased to 100 °C, with slight decreases in the intensity of Soret and visible bands (Fig. 7B). Therefore, the T_m was estimated to be higher than 100 °C, in agreement with the CD result. These results indicate that with an additional intramolecular disulfide bond of C15–C120, A15C Ngb exhibits extremely high thermal stability, and retains almost half α-helix structure at 100 °C, as well as most of the overall protein structure, where the heme was stabilized in the heme pocket.

Kinetic studies

With an enhanced protein stability of A15C Ngb, we were further interested in testing the functional consequence of the formation of an additional disulfide bond. We first studied the autoxidation of A15C Ngb and compared to that of WT Ngb. As shown in Fig. 8A, the visible bands of the oxy-form (542 nm and 576 nm) decrease in intensity over time due to the autoxidation. The plot of the absorption change at 542 nm *versus* time obeys a single-exponential decay function (Fig. 8A, inset). The rate constant of autoxidation was determined to be 5.5×10^{-4} s^{-1} for A15C Ngb at pH 7.0, 25 °C, which is ~1.38-fold higher than that for WT Ngb under the identical conditions (4.0×10^{-4} s^{-1}). Note that these values (pH 7.0, 25 °C) are lower than that determined for WT Ngb in previous studies at higher pH value (2.8×10^{-3} s^{-1}, pH 7.5, 25 °C)[59] or higher temperature (3.8×10^{-3} s^{-1}, pH 7.4, 37 °C).[55]

Moreover, we determined the O_2 release rate using stopped-flow spectroscopy upon reaction of oxy-Ngbs (5 μM) with sodium dithionite (1 mM) in 100 mM potassium phosphate buffer (pH 7.0) at 25 °C. As shown in Fig. 8B, the oxy-form (542 nm and 576 nm) of A15C Ngb was rapidly converted to the reduced form (529 nm and 559 nm). From the plot of the absorption change for the oxy-form at 542 nm *versus* time (Fig. 8B, inset), the rate constant of O_2 release was calculated to be 0.32 ± 0.01 s^{-1}, which is ~1.39-fold higher than that for WT Ngb under the identical conditions (0.23 ± 0.01 s^{-1}). These observations suggest that the formation of a second disulfide bond of C15–C120 in A15C Ngb slightly alters the protein function, with an increase in the rate of O_2 release by ~1.4-fold.

It was interesting to observe that A15C Ngb with a more stable structure releases O_2 easier than that of WT Ngb. The explanation for this observation may include two aspects. (1) The *de novo* disulfide bond of C15–C120 is remote from the heme center, *i.e.*, ~23 Å according to the modeling structure (Fig. 1A). It may leads to long-range structural changes that impact on the heme iron coordination, as suggested by Astudillo *et al.* in study of C120S Ngb mutant;[53] (2) the free C120 may interfere with the heme reduction process and thereby the O_2 release. In a previous study, Hirota *et al.* introduced a cysteine to various sites on the surface of sperm whale Mb, and showed that the heme reduction rate constant decreased in general as the heme-cysteine distance was increased.[60] Therefore, the formation of C15–C120 disulfide bond in A15C Ngb may eliminate such an effect. Note that although dithionite is commonly

used to determine O_2 release of heme proteins *in vitro*,[39,61] for *in vivo* reduction of Ngb, many biological reductants could be involved, such as GSH and redox partners Cyt b_5 and Cyt *c*.[62,63]

Conclusions

Ngb is a promising model protein for heme protein design, and in order to protect the free Cys120 in human Ngb and to enhance the protein stability, we rationally designed an additional disulfide of Cys15–Cys120 in Ngb by introduction of Cys15 in the vicinity of Cys120. As predicted by molecular modeling, Cys15 and Cys120 formed an intramolecular disulfide bond, which was confirmed experimentally by ESI-MS analysis, with WT Ngb as a control. The formation of Cys15–Cys120 disulfide bond was found to have minimal structural alterations of Ngb, meanwhile, it enhanced both chemical and pH stabilities with respect to those of WT Ngb with a single native disulfide bond of Cys46–Cys55. Thermal-induced unfolding studies revealed that A15C Ngb retained most of the overall protein structure as high as 100 °C, indicating an ultra-high thermal stability. In addition, the disulfide bond of Cys15–Cys120 remote from the heme center has only slight effects on protein function, such as an increase in the rate of O_2 release by ~1.4-fold. These results suggest that an additional disulfide can be rationally designed in Ngb, which plays a crucial role in protein stabilization. Moreover, this study lays the groundwork for further investigation of the structure and function of Ngb, as well as for the design of other functional heme proteins, based on the scaffold of A15C Ngb with an enhanced stability.

Materials and methods

Protein preparation

The pET3a plasmid DNA containing the gene of human Ngb was a gift from Prof. T. Burmester, Gutenberg University of Mainz, Germany. Ngb was expressed in *E. Coli.* BL21(DE3) cells and purified as previously reported.[45] The A15C Ngb gene was constructed using the QuikChange Site Directed Mutagenesis Kit (Stratagene) with two primers: forward, 5′-CAG AGC TGG CGG TGT GTG AGC CGC AGC-3′, and reverse, 5′-GCT GCG GCT CAC ACA CCG CCA GCT CTG-3′. The mutation was confirmed by DNA sequencing assay, and the mutant was expressed and purified using the same procedure as that for WT Ngb.[45]

Molecular modeling studies

The initial structure of A15C Ngb was constructed based on the X-ray crystal structure of human Ngb (PDB code 4MPM, molecule A[48]) using program VMD 1.9. A patch of disulfide bond was applied to Cys46–Cys55 and Cys15–Cys120, respectively. The protein was solvated in a cubic box of TIP3 water, which extended 10 Å away from any given protein atom. Counter ions (Na^+ and Cl^-) were further added to obtain the physiological ionic strength of 0.15 M by using the autoionize plug-in of VMD 1.9.[64] The resulting system was minimized with NAMD2.9 (Nanoscale Molecular Dynamics),[65] using 50 000 minimization steps with conjugate gradient method at 0 K, and equilibrated for 15 000 000 molecular dynamics steps (1 fs per step, 15 ns in total) at 310 K, then further minimized for 50 000 steps at 0 K. Visualization and data analysis were done with VMD 1.9.

UV-Vis and CD studies

UV-Vis spectra of A15C Ngb and WT Ngb were collected on an Agilent 8453 spectrometer in 100 mM potassium phosphate buffer (pH 7.0) at 25 °C. Circular dichroism (CD) spectra were collected on a Jasco 1500 spectropolarimeter equipped with a MCB-100 mini circulation bath (25 °C), using a cuvette with a path length of 0.1 cm and 1 cm for 190–250 nm and 250–700 nm, respectively. The protein concentrations of WT Ngb and A15C Ngb were determined with an extinction coefficient of $\varepsilon_{413\ nm} = 129\ mM^{-1}\ cm^{-1}$,[49] and $\varepsilon_{413\ nm} = 139\ mM^{-1}\ cm^{-1}$, respectively, as calculated using the standard hemochromogen method.[66]

Mass spectrometry

Protein mass spectrum was measured on G2-XS QToF mass spectrometer (Waters). The desalted protein solution was mixed with 50% acetonitrile solution (acetonitrile : water, 1 : 1) containing 1% formic acid, and transferred into the mass spectrometer chamber for measurement by a direct injection method without performing the liquid chromatography under positive mode. The multiple *m*/*z* peaks were transformed to the protein molecular weight by using software MaxEnt1. For reduction studies, the reducing agent tris-(2-carboxyethyl)-phosphine (TCEP) was added to the protein solution at a final concentration of 10 mM, and the mixture was cultured at 37 °C for 30 min before mass measurements.

Gdn·HCl-induced unfolding studies

Gdn·HCl-induced unfolding of A15C Ngb was studied by Agilent 8453 spectrometer. 10 μL of 2 mM protein sample was added into 2 mL of a guanidine hydrochloride (Gdn·HCl) solution (pH 7.0) with various concentrations (0–6.0 M). After incubation for 30 min, the UV-Vis spectrum was recorded. Control experiment was performed for WT Ngb under the same conditions. The unfolding transition was monitored at different Gdn·HCl concentrations through the changes of the absorbance of the Soret band. The denaturation midpoint (C_m) was calculated by fitting the absorbance of Soret band *versus* the concentration of Gdn·HCl to a two-state Boltzmann function (eqn (1)).

$$A = A_2 + (A_1 - A_2)/(1 + e^{(C-C_m)/dC}) \quad (1)$$

Here, A is the absorbance of Soret band; A_1 and A_2 are the initial and final absorbance of Soret band, respectively; C is the concentration of Gdn·HCl; C_m is the concentration of Gdn·HCl at midpoint of denaturation.

Acid-induced unfolding studies

The acidic stability of A15C Ngb upon pH-induced unfolding was carried out on an Agilent 8453 spectrometer using a cell with a path length of 1 cm. The temperature was controlled at 25 °C with a circulating bath. The protein sample was titrated with increasing amounts of 10 M HCl to adjust the pH values. After incubation at different pH values for 10 min, the UV-Vis spectrum was recorded. Control experiment was performed for WT Ngb under the same conditions. The denaturation midpoint was calculated by fitting the absorbance of Soret band *versus* the pH values to a two-state Boltzmann function (eqn (2)).

$$A = A_2 + (A_1 - A_2)/(1 + e^{(X-X_0)/dX}) \quad (2)$$

Here, A is the absorbance of Soret band; A_1 and A_2 are the initial and final absorbance of Soret band, respectively; X is the pH value; X_0 is the pH at midpoint of denaturation.

Thermal-induced unfolding studies

Thermal-induced unfolding studies of WT Ngb and A15C Ngb were performed with a Jasco 1500 spectropolarimeter equipped with a MCB-100 minicirculation bath. The protein was dissolved in potassium phosphate buffer (100 mM, pH 7.0) using a cuvette with a path length of 0.1 cm and 1 cm with their corresponding covers. The temperature was increased stepwise over the range of 25–100 °C. At each temperature, the protein sample was allowed to equilibrate for 10 min before collecting the CD spectrum (190–250 nm) at a speed of 100 nm min^{-1} for five times, and the UV-Vis spectrum (250–700 nm) at a speed of 200 nm min^{-1} for six times. The denaturation midpoint (T_m) was calculated by fitting the ellipticity at 222 nm or the absorbance of Soret band *versus* the temperature to a two-state Boltzmann function (eqn (3)).

$$A = A_2 + (A_1 - A_2)/(1 + e^{(T-T_m)/dT}) \quad (3)$$

Here, A is the absorbance of Soret band; A_1 and A_2 are the initial and final absorbance of Soret band, respectively; T is the temperature.

Kinetic studies

The autoxidation rates of oxy-Ngb and oxy-A15C Ngb were determined using an Agilent 8453 spectrometer. The ferric protein was reduced by excess dithionite, which was removed from the solution by a PD-10 column (GE Healthcare). The reduced protein was then diluted into O_2-saturated 100 mM potassium phosphate (pH 7.0) to generate the oxy-form protein. The changes in intensity of the oxy-form band at 542 nm were monitored for 60 min at 25 °C, and fitted to a single-exponential decay function. The O_2 dissociation rates of oxy-Ngb and oxy-A15C Ngb were determined using a dual mixing stopped-flow spectrophotometer (SF-61DX2 Hi-Tech KinetAsyst™). The prepared oxy-Ngbs (10 μM protein in 100 mM potassium phosphate, pH 7.0) was mixed with an equal volume of 1 mM sodium dithionite. The changes in intensity of the oxy-form band at 542 nm were monitored for 10 s at 25 °C, and fitted to a single-exponential decay function to obtain the observed rate constant (k_{obs}, s^{-1}).

Conflicts of interest

There are no conflicts to declare.

Acknowledgements

We gratefully thank Prof. T. Burmester of the Gutenberg University of Mainz, Germany, for graciously providing the gene of human Ngb. This work was supported by the National Natural Science Foundation of China, NSFC (31370812; 21701081) and Hunan province college students research learning and innovative experiment project (136).

References

1 Y. Lu, N. Yeung, N. Sieracki and N. M. Marshall, *Nature*, 2009, **460**, 855–862.
2 J. Du, M. Sono and J. H. Dawson, *Coord. Chem. Rev.*, 2011, **255**, 700–716.
3 U. Liebl, J.-C. Lambry and M. H. Vos, *Biochim. Biophys. Acta*, 2013, **1834**, 1684–1692.
4 T. L. Poulos, *Chem. Rev.*, 2014, **114**, 3919–3962.
5 J. Liu, S. Chakraborty, P. Hosseinzadeh, Y. Yu, S. Tian, I. Petrik, A. Bhagi and Y. Lu, *Chem. Rev.*, 2014, **114**, 4366–4469.
6 P. C. E. Moody and E. L. Raven, *Acc. Chem. Res.*, 2018, **51**, 427–435.
7 Y.-W. Lin, E. B. Sawyer and J. Wang, *Chem.–Asian J.*, 2013, **8**, 2534–2544.
8 I. D. Petrik, J. Liu and Y. Lu, *Curr. Opin. Chem. Biol.*, 2014, **19**, 67–75.
9 K. Oohora and T. Hayashi, *Curr. Opin. Chem. Biol.*, 2014, **19**, 154–161.
10 O. Shoji and Y. Watanabe, *J. Biol. Inorg Chem.*, 2014, **19**, 529–539.
11 F. Nastri, M. Chino, O. Maglio, A. Bhagi-Damodaran, Y. Lu and A. Lombardi, *Chem. Soc. Rev.*, 2016, **45**, 5020–5054.
12 Y.-W. Lin, *Coord. Chem. Rev.*, 2017, **336**, 1–27.
13 S. Hirota and Y. W. Lin, *J. Biol. Inorg Chem.*, 2018, **23**, 7–25.
14 Y. Yu, C. Hu, L. Xia and J. Wang, *ACS Catal.*, 2018, **8**, 1851–1863.
15 F. Schwizer, Y. Okamoto, T. Heinisch, Y. Gu, M. M. Pellizzoni, V. Lebrun, R. Reuter, V. Kohler, J. C. Lewis and T. R. Ward, *Chem. Rev.*, 2018, **118**, 142–231.
16 E. N. Mirts, I. D. Petrik, P. Hosseinzadeh, M. J. Nilges and Y. Lu, *Science*, 2018, **361**, 1098–1101.
17 L.-L. Yin, H. Yuan, C. Liu, B. He, S.-Q. Gao, G.-B. Wen, X. Tan and Y.-W. Lin, *ACS Catal.*, 2018, **8**, 9619–9624.
18 M. Lehmann and M. Wyss, *Curr. Opin. Biotechnol.*, 2001, **12**, 371–375.
19 A. Gershenson and F. H. Arnold, *Genet. Eng.*, 2000, **22**, 55–76.
20 T. J. Magliery, *Curr. Opin. Struct. Biol.*, 2015, **33**, 161–168.
21 L. J. Perry and R. Wetzel, *Science*, 1984, **226**, 555.

22 R. Wetzel, L. J. Perry, W. A. Baase and W. J. Becktel, *Proc. Natl. Acad. Sci. U. S. A.*, 1988, **85**, 401–405.
23 M. Matsumura, G. Signor and B. W. Matthews, *Nature*, 1989, **342**, 291–293.
24 J. M. Chalker, G. J. Bernardes, Y. A. Lin and B. G. Davis, *Chem.–Asian J.*, 2009, **4**, 630–640.
25 J. Lee and M. Blaber, *J. Mol. Biol.*, 2009, **393**, 128–139.
26 A. A. Dombkowski, K. Z. Sultana and D. B. Craig, *FEBS Lett.*, 2014, **588**, 206–212.
27 T. Liu, Y. Wang, X. Luo, J. Li, S. A. Reed, H. Xiao, T. S. Young and P. G. Schultz, *Proc. Natl. Acad. Sci. U. S. A.*, 2016, **113**, 5910–5915.
28 C. Colas and P. R. Ortiz de Montellano, *Chem. Rev.*, 2003, **103**, 2305–2332.
29 Y.-W. Lin, *Biochim. Biophys. Acta*, 2015, **1854**, 844–859.
30 Y.-W. Lin, *Arch. Biochem. Biophys.*, 2018, **641**, 1–30.
31 P. D. Barker, J. C. Ferrer, M. Mylrajan, T. M. Loehr, R. Feng, Y. Konishi, W. D. Funk, R. T. MacGillivray and A. G. Mauk, *Proc. Natl. Acad. Sci. U. S. A.*, 1993, **90**, 6542–6546.
32 Y.-W. Lin, W.-H. Wang, Q. Zhang, H.-J. Lu, P.-Y. Yang, Y. Xie, Z.-X. Huang and H.-M. Wu, *ChemBioChem*, 2005, **6**, 1356–1359.
33 S. Hu, B. He, K.-J. Du, X.-J. Wang, S.-Q. Gao and Y.-W. Lin, *ChemistryOpen*, 2017, **6**, 325–330.
34 P. D. Barker, E. P. Nerou, S. M. V. Freund and I. M. Fearnley, *Biochemistry*, 1995, **34**, 15191–15203.
35 C. L. Metcalfe, O. Daltrop, S. J. Ferguson and E. L. Raven, *Biochem. J.*, 2007, **408**, 355–361.
36 H.-M. Cheng, H. Yuan, X.-J. Wang, J.-K. Xu, S.-Q. Gao, G.-B. Wen, X. Tan and Y.-W. Lin, *J. Inorg. Biochem.*, 2018, **182**, 141–149.
37 C. L. Metcalfe, M. Ott, N. Patel, K. Singh, S. C. Mistry, H. M. Goff and E. L. Raven, *J. Am. Chem. Soc.*, 2004, **126**, 16242–16248.
38 S. L. Rice, M. R. Preimesberger, E. A. Johnson and J. T. Lecomte, *J. Inorg. Biochem.*, 2014, **141**, 198–207.
39 D.-J. Yan, W. Li, Y. Xiang, G.-B. Wen, Y.-W. Lin and X. Tan, *ChemBioChem*, 2015, **16**, 47–50.
40 D.-J. Yan, H. Yuan, W. Li, Y. Xiang, B. He, C.-M. Nie, G.-B. Wen, Y.-W. Lin and X. Tan, *Dalton Trans.*, 2015, **44**, 18815–18822.
41 T. Uchida, M. Unno, K. Ishimori and I. Morishima, *Biochemistry*, 1997, **36**, 324–332.
42 L.-B. Wu, H. Yuan, H. Zhou, S.-Q. Gao, C.-M. Nie, X. Tan, G.-B. Wen and Y.-W. Lin, *Arch. Biochem. Biophys.*, 2016, **600**, 47–55.
43 L.-L. Yin, H. Yuan, K.-J. Du, B. He, S.-Q. Gao, G.-B. Wen, X. Tan and Y.-W. Lin, *Chem. Commun.*, 2018, **54**, 4356–4359.
44 T. Burmester, B. Weich, S. Reinhardt and T. Hankeln, *Nature*, 2000, **407**, 520–523.
45 S. Dewilde, L. Kiger, T. Burmester, T. Hankeln, V. Baudin-Creuza, T. Aerts, M. C. Marden, R. Caubergs and L. Moens, *J. Biol. Chem.*, 2001, **276**, 38949–38955.
46 D. Hamdane, L. Kiger, S. Dewilde, B. N. Green, A. Pesce, J. Uzan, T. Burmester, T. Hankeln, M. Bolognesi, L. Moens and M. C. Marden, *J. Biol. Chem.*, 2003, **278**, 51713–51721.
47 L. Astudillo, S. Bernad, V. Derrien, P. Sebban and J. Miksovska, *Biophys. J.*, 2010, **99**, L16–L18.
48 B. G. Guimaraes, D. Hamdane, C. Lechauve, M. C. Marden and B. Golinelli-Pimpaneau, *Acta Crystallogr., Sect. D: Biol. Crystallogr.*, 2014, **70**, 1005–1014.
49 S. Nicolis, E. Monzani, C. Ciaccio, P. Ascenzi, L. Moens and L. Casella, *Biochem. J.*, 2007, **407**, 89–99.
50 M. Tiso, J. Tejero, S. Basu, I. Azarov, X. Wang, V. Simplaceanu, S. Frizzell, T. Jayaraman, L. Geary, C. Shapiro, C. Ho, S. Shiva, D. B. Kim-Shapiro and M. T. Gladwin, *J. Biol. Chem.*, 2011, **286**, 18277–18289.
51 A. Bocahut, V. Derrien, S. Bernad, P. Sebban, S. Sacquin-Mora, E. Guittet and E. Lescop, *J. Biol. Inorg Chem.*, 2013, **18**, 111–122.
52 S. Trashin, M. de Jong, E. Luyckx, S. Dewilde and K. De Wael, *J. Biol. Chem.*, 2016, **291**, 18959–18966.
53 L. Astudillo, S. Bernad, V. Derrien, P. Sebban and J. Miksovska, *Biochemistry*, 2012, **51**, 9984–9994.
54 I. Azarov, L. Wang, J. J. Rose, Q. Xu, X. N. Huang, A. Belanger, Y. Wang, L. Guo, C. Liu, K. B. Ucer, C. F. McTiernan, C. P. O'Donnell, S. Shiva, J. Tejero, D. B. Kim-Shapiro and M. T. Gladwin, *Sci. Transl. Med.*, 2016, **8**, 368ra173.
55 J. Tejero, C. E. Sparacino-Watkins, V. Ragireddy, S. Frizzell and M. T. Gladwin, *Biochemistry*, 2015, **54**, 722–733.
56 H.-X. Liu, L. Li, B. He, S.-Q. Gao, G.-B. Wen and Y.-W. Lin, *Dalton Trans.*, 2018, **47**, 10847–10852.
57 E. J. Moore, D. Zorine, W. A. Hansen, S. D. Khare and R. Fasan, *Proc. Natl. Acad. Sci. U. S. A.*, 2017, **114**, 12472–12477.
58 H. Zhang, C. Kenaan, D. Hamdane, G. H. Hoa and P. F. Hollenberg, *J. Biol. Chem.*, 2009, **284**, 25678–25686.
59 A. Fago, C. Hundahl, S. Dewilde, K. Gilany, L. Moens and R. E. Weber, *J. Biol. Chem.*, 2004, **279**, 44417–44426.
60 S. Hirota, K. Azuma, M. Fukuba, S. Kuroiwa and N. Funasaki, *Biochemistry*, 2005, **44**, 10322–10327.
61 S. Nagao, H. Osuka, T. Yamada, T. Uni, Y. Shomura, K. Imai, Y. Higuchi and S. Hirota, *Dalton Trans.*, 2012, **41**, 11378–11385.
62 P. Ascenzi, A. di Masi, L. Leboffe, M. Fiocchetti, M. T. Nuzzo, M. Brunori and M. Marino, *Mol. Aspects Med.*, 2016, **52**, 1–48.
63 M. Fiocchetti, M. Cipolletti, V. Brandi, F. Polticelli and P. Ascenzi, *J. Mol. Recognit.*, 2017, e2654.
64 W. Humphrey, A. Dalke and K. Schulten, *J. Mol. Graphics*, 1996, **14**(33–38), 27–38.
65 L. Kalé, R. Skeel, M. Bhandarkar, R. Brunner, A. Gursoy, N. Krawetz, J. Phillips, A. Shinozaki, K. Varadarajan and K. Schulten, *J. Comput. Phys.*, 1999, **151**, 283–312.
66 M. Morrison and S. Horie, *Anal. Biochem.*, 1965, **12**, 77–82.